Research Square

Preprints are preliminary reports that have not undergone peer review.
They should not be considered conclusive, used to inform clinical practice,
or referenced by the media as validated information.

A Surge of Confidence: Validation of High-Frequency Satellite Altimetry for Storm Surge Detection

Jemma Philpotts Johnson

jemma.johnson@tum.de

Deutsches Geodätisches Forschungsinstitut, Technische Universität München (DGFI-TUM)

Michael G. Hart-Davis

Deutsches Geodätisches Forschungsinstitut, Technische Universität München (DGFI-TUM)

Björn Backeberg

Deltares

Christian Schwatke

Deutsches Geodätisches Forschungsinstitut, Technische Universität München (DGFI-TUM)

Marcello Passaro

Deutsches Geodätisches Forschungsinstitut, Technische Universität München (DGFI-TUM)

Article

Keywords:

Posted Date: November 23rd, 2026

DOI: https://doi.org/10.21203/rs.3.rs-11622705/v1

License: This work is licensed under a Creative Commons Attribution 4.0 International License.
Read Full License

Additional Declarations: No competing interests reported.

A Surge of Confidence: Validation of High-Frequency Satellite Altimetry for Storm Surge Detection

Jemma Philpotts Johnson[1*], Michael G. Hart-Davis[1], Björn Backeberg[2,3], Christian Schwatke[1], and Marcello Passaro[1]

[1]Deutsches Geodätisches Forschungsinstitut, Technische Universität München (DGFI-TUM), Germany
[2]Deltares, Delft, Netherlands
[3]Nansen Environmental and Remote Sensing Center, Bergen, Norway
[*]Corresponding author: jemma.johnson@tum.de

ABSTRACT

Storm surges are a primary driver of coastal flooding and one of the most significant natural hazards affecting low-lying communities worldwide. This study evaluates the potential of high-rate coastal altimetry for storm surge detection by validating the satellite-derived observations against tide gauge measurements and sea level estimates from the Global Tide and Surge Model (GTSM). The altimetry data were spatially matched to tide gauge locations, and a filtering framework was developed to isolate a more realistic coastal sea level signal from the noisy raw observations. Between 2002 and 2020, over 1,500 storm surge events were matched with altimetry observations across more than 500 tide gauge locations. Altimetry generally underestimates sea level relative to tide gauge measurements, with a mean difference of approximately 20 cm and a correlation coefficient exceeding 0.7. The results also show that this level of performance is independent of the alongshore distance between tide gauges and the altimetry track within a 50 km threshold distance. Comparison with the GTSM showed strong correlations between model estimates at nearest-to-coast satellite and gauge locations. Comparison of GTSM sea level estimates with altimetry observations yielded a correlation coefficient exceeding 0.9 and a mean difference of 14 cm. Investigation of individual gauges also showed that tide gauge processing errors can introduce false storm surge signals and contribute to the gauge-altimetry disagreement. These findings demonstrate that the pre- and post-processing approach can provide a reliable altimetry record of storm surge activity close to the coast, contrary to widespread concerns about the quality of high-rate coastal altimetry data. This also emphasizes the potential of these data for systematically validating GTSM predictions in areas without tide gauges. Discrepancies between tide gauge observations and both altimetry-derived and GTSM-estimated sea levels during extreme sea level events underscore the need for a better understanding of the factors influencing how extreme sea levels are represented by observational and modeling approaches.

Introduction

A storm surge is an extreme rise in sea level above the predicted tide, caused primarily by the combined effects of wind stress, low atmospheric pressure, and wave processes associated with intense weather systems[1]. The spatial scale and severity of a surge can vary substantially as a result of both storm characteristics and local coastal conditions such as bathymetry and coastal morphology[2]. In particular, when a storm surge occurs during high tide, the rising sea level can reach extreme peaks, generating a rapid influx of nearshore water capable of destroying structures and inundating coastal communities[3]. Consequently, the human toll of these events can be catastrophic. Storm surges are responsible for roughly 50% of all hurricane fatalities along the North American Atlantic coast[4] and are estimated to cause approximately 13,000 fatalities annually across the globe[5]. Storm surges occur worldwide, yet a comprehensive global system for observing and monitoring them remains limited. With approximately 40% of the global population living within 100 km of a coastline[6], the socioeconomic impacts of coastal flooding are expected to intensify as population growth coincides with sea level rise, making accurate observation of storm surges critical for hazard assessment and risk mitigation.

Storm surges have been extensively studied using a variety of remote sensing techniques and in situ data. Numerous analyses have focused on monitoring storm surges in specific geographic regions, including the Chinese coast[7] and the Bay of Bengal[8]. Conventional (1 Hz) satellite altimetry has also proven successful in observing individual storm surge events, including those associated with Hurricane Igor[9] and Hurricane Sandy[10]. The potential of satellite-derived data for storm surge monitoring has also motivated efforts to develop more comprehensive approaches for global analyses. The ESA eSurge project was established to develop a globally applicable system for storm surge monitoring and forecasting by integrating satellite observations into storm surge models[11]. However, as the eSurge project is no longer active, there remains an opportunity for further research to advance global storm surge detection, particularly through emerging coastal altimetry techniques.

Since the nineteenth century, sea level has been continuously monitored using tide gauges, which provide long-term, reliable records of sea level at fixed nearshore locations[12]. While these records are foundational to coastal sea level observation, tide gauges are inherently local, with differences in temporal coverage, instrumentation, and vertical reference levels limiting their usability for larger-scale sea level analyses[13]. Furthermore, the global tide gauge network is unevenly distributed, with a majority of instruments stationed along North American and European coasts (Figure 1). This inequity leaves critical gaps in sea level observations across many coastal regions, particularly in the Southern Hemisphere, where coastlines are often sparsely monitored or entirely ungauged.

Numerical models can help address some of these limitations by estimating sea level across larger domains, including in regions where tide gauge observations are unreliable. However, the greater spatial and temporal scale of model output data does not necessarily provide a more accurate representation of local coastal conditions. Numerical models are sensitive to their underpinning assumptions, grid resolution, and the quality of forcing fields[14]. These factors can introduce uncertainties that can limit the ability of models to accurately reproduce localized processes, particularly sea level extremes. Rather than serving as alternatives to one another, numerical models and tide gauges provide complementary data that together support a more comprehensive and reliable understanding of coastal sea level dynamics.

Satellite radar altimetry offers a space-based approach to sea level observation, providing over three decades of continuous, global measurements. Altimeters determine sea level by measuring the round-trip travel time of radar pulses emitted by the satellite and reflected off the ocean surface[15]. The power of the returning signal is recorded as a waveform and processed, or retracked, to derive the satellite-to-surface range[16]. Reflections from land, shallow bathymetry, and calm coastal waters, as discussed by Cipollini et al. (2017)[13], can distort returned waveforms and compromise the performance of standard retracking algorithms developed for open-ocean conditions. This reduces the reliability of conventional satellite altimetry in coastal zones. Furthermore, standard atmospheric and geophysical corrections, which mitigate signal delays and physical influences to improve sea level estimates, become less reliable near the coast which creates additional uncertainties. Consequently, altimetry-derived sea level data within approximately 10-50 km of the coast have historically been discarded, limiting the application of satellite altimetry for coastal ocean studies[13].

These challenges have motivated innovation in the field of coastal altimetry, leading to specialized retracking and processing methods designed to recover more reliable nearshore data. For example, Adaptive Leading Edge Subwaveform (ALES)[16] is a retracking algorithm that adaptively adjusts the segment of the waveform used to estimate the sea level based on significant wave height. The typical data rate of the averaged waveforms is 20 Hz for most of the altimetry missions, which corresponds to a spatial resolution of approximately 300 m[16]. ALES data has been incorporated into several post-processing techniques such as X-TRACK, a processing system that applies coastal-specific data filtering and corrections tailored to the nearshore zone[17]. While altimetry data are typically averaged to a 1-Hz sampling rate for open-ocean applications, retaining the original 20-Hz sampling provides higher spatial resolution, improving the observation of smaller-scale coastal sea level variability, which is particularly valuable for studying storm surges.

This study aims to assess the ability of satellite altimetry to detect storm surges on a global scale. The primary objectives are to evaluate: (1) the extent to which storm surges are discernible in high-frequency altimetry data; (2) how altimetry processing and filtering can be optimized to improve the nearshore signal and maximize the accuracy of the storm surge detections; and (3) the factors contributing to discrepancies between tide gauge observations, satellite altimetry, and model estimates. To address these objectives, high-rate coastal altimetry data are validated against tide gauge measurements and simulations from the Global Tide and Surge Model (GTSM).

Results and Discussion

Storm surges were detected using sea level anomaly (SLA) and dynamic atmospheric correction (DAC) observations from two coastal altimetry datasets: the ESA Sea Level CCI along-track 10-day, 20-Hz dataset (AX) and the DGFI-TUM Open Altimeter Database (ADB)[18]. Altimetry-derived storm surge captures were validated using tide gauge records. Further details on these datasets and the altimetry variables used in the analysis are provided in the Data and Methodology section. Across the study domain, 1,629 storm surges were captured by AX altimetry at 540 tide gauge locations and 1,396 events at 505 locations with the ADB dataset. The variation in the number of storm surge events detected by the two altimetry products stems from their respective processing and data-flagging procedures.

The spatial distribution of tide gauges included in the analysis (Figure 2a) reveals substantial variation in the number of unique storm surge days identified at each location, with many gauges recording more than 500 days, while others recording fewer than 100. The number of days on which altimetry data were available during the time of a storm surge is noticeably smaller (Figure 2b). At many locations, fewer than 10 storm surges coincide with a satellite overpass. Of the more than 200,000 total unique storm surge days identified from the tide gauge records, only approximately 0.6% align with AX altimetry and 0.5% by ADB, highlighting the challenge of temporal alignment. The satellites included in this study revisit a given location approximately every 10 days, and each overpass within the 50 km colocation radius lasts only a few seconds. Consequently,

only a small proportion of recorded storm surge events coincide with available altimetry observations and are included in the comparison. This constraint demonstrates the need to increase the availability of reliable altimetry data processed for coastal applications and to expand the network of validation data.

Comparison of Altimetry-derived and Tide Gauge Measurements of Storm Surges

To assess the accuracy of altimetry-derived storm surge measurements, the difference between the nearest-to-coast (NTC) filtered SLA+DAC observation and the coincident tide gauge measurement was computed for all storm surge captures. Figure 3 shows these differences in dark blue, with the events ordered from smallest to largest difference. The red point series indicates the storm surge sea level measured by the tide gauge, while the light blue series shows the corresponding altimetry value.

For the majority of storm surge events, the two systems show high agreement in the observed storm surge sea level, with the altimetry-gauge difference remaining below 0.5 m until approximately event 1400 in the AX dataset and event 1200 in the ADB dataset. For AX altimetry, the mean difference between the tide gauge and satellite-based sea level is 0.2031 m, with a median of 0.1154 m. For ADB, the corresponding mean and median differences are 0.1710 m and 0.0900 m, respectively. Considering only events observed by both datasets, the AX mean and median increase to 0.2108 m and 0.1202 m. In both datasets, the median difference is lower than the mean, indicating that more events exhibit closer gauge-altimetry agreement, while a smaller subset of events with large differences raises the overall average difference.

Previous studies reported differences between altimetry-derived and tide gauge-measured storm surge levels of 0.14 m, averaged across five altimetry-gauge comparisons[9], and 0.1 m for a single comparison[10]. In the AX dataset, the absolute difference was below 0.1 m for 566 events and below 0.14 m for 758 events. Similarly, in the ADB dataset, 475 events had differences below 0.1 m, while 629 events had differences below 0.14 m. Although the mean differences found in this work are higher than the mean differences of previous studies, this study includes more than 1,000 storm surge events across hundreds of tide gauge locations, capturing a wider range of coastal conditions and introducing more potential sources of uncertainty than single-storm case studies.

At the upper end of the distribution, differences between the tide gauge and the altimetry are significant, with altimetry-derived sea level observations approaching zero while the tide gauge records several meters of surge. The following section examines these cases of particularly large discrepancies to assess the validity and possible causes of the error.

The RMSE values for the tide gauge-AX and tide gauge-ADB comparisons are 0.5513 m and 0.6145 m, respectively, both of which are larger than the altimetry-gauge RMSE of 0.188 m reported by Lobeto et al. (2024)[19]. However, these higher errors should again be interpreted in the context of differences in study design and gauge selection. These results include approximately four times as many tide gauges as the Lobeto et al. (2024)[19] study. Lobeto et al. (2024)[19] also excluded gauges located in rivers and sheltered environments, which this study did not. The higher RMSE observed here can therefore reflect the inclusion of gauges affected by more complex local hydrodynamics, rather than poorer altimetry performance.

Altimetry underestimates sea level relative to the tide gauge for 72.86% of recorded storm surges with AX and 67.12% with ADB. This trend is consistent with previous studies reporting that satellite altimetry tends to underestimate extreme coastal sea levels due to irregular satellite sampling, differences in the spatiotemporal resolution of satellite and tide gauge observations, and smoothing effects that limit the physical representation of storm conditions[19]. Overestimation cases are observed for approximately 30% of events in both datasets, and their underlying causes remain unclear. Further investigation is needed to determine whether these overestimates occur due to physical effects, such as local coastal dynamics, or due to errors introduced by data processing.

The distributions of differences between tide gauge and altimetry are shown in Figure 4. For both datasets, the majority of differences are concentrated within ± 0.5 m. Both distributions are positively skewed and therefore cannot be adequately characterized by a normal distribution. Consequently, the 5th and 95th percentiles were used to identify unusually large differences between tide gauge and altimetry measurements. In the AX dataset, 24 gauges have more than 50% of their gauge-altimetry differences outside this percentile range, compared with 30 gauges in the ADB dataset. Of these, 16 are common to both datasets.

Investigating Cases with Significant Gauge-Altimetry Disagreement

Figure 5 presents storm surge validation results for the 16 tide gauges exhibiting consistently low agreement with both AX and ADB altimetry. At these locations, tide gauges record extreme sea levels during events for which the corresponding satellite observations show very low or negative SLA+DAC values, resulting in discrepancies that exceed 5 m in some cases. Examination of the intermediate stages of tide gauge preprocessing (Supplementary Figures 1–4) reveals that the low agreement for these 16 gauges can be traced to several causes. The tide gauge preprocessing and the harmonic analysis (HA) used for tidal prediction are described in *Tide Gauge Data and Processing* of the Data and Methodology section.

Gauges (k), (l), (m), and (o) contain frequent gaps and extreme outliers in the raw sea level records that propagate through subsequent processing stages. These gauges can therefore be excluded from the results because their derived surges are not

reliable references for validating satellite altimetry. Gauges (i) and (j) are located in rivers. These gauges can also be excluded, as their locations are less representative of the coastal environments targeted in this study.

The remaining gauges in Supplementary Figures 1–4 have more continuous records, and their corrected sea levels and predicted tides are consistent with the expected variability. However, various outliers persist through the processing stages, affecting the HA and the derived surge. Because storm surge events are identified from the surge series using a 3σ threshold, residual outliers can inflate the threshold and cause extreme errors to be flagged as storm surges while genuine surge events go undetected.

In addition to data quality, the geographical distribution of the 16 low gauge-altimetry agreement tide gauges also presents a challenge. Supplementary Figure 5 shows that many of these gauges are located in estuaries, where interactions between tidal propagation and river dynamics can introduce nonlinearities into the tidal signal[20]. These processes can reduce the effectiveness of the HA method, requiring alternative approaches for tidal prediction to better account for nonlinear and time-varying dynamics. The following case study examines one of these gauges in greater detail, focusing on the effect of modifying the tide gauge processing procedure on gauge-altimetry agreement.

Tide gauge specific processing: Mumbles UK Case Study

The *mumbles-mum-gbr-bodc* tide gauge is located in the Bristol Channel, an estuarine environment where tidal prediction is affected by complex local hydrodynamics. For each storm surge validation result (Supplementary Figure 6), the tide gauge records surge levels exceeding 1 m, whereas the corresponding altimetry observations indicate low or negative sea level anomalies. All captured storm surge events occur in 2018.

Inspection of the raw (Supplementary Figure 1) and corrected tide gauge record (Supplementary Figure 2) reveals an anomalous section of sea level variability around 2018, when the gauge exhibits an unusually small signal relative to the approximately -5 to 5 m range of the corrected sea level record. This anomaly propagates into the predicted tide (Supplementary Figure 3) and the surge (Supplementary Figure 4), with a segment of data around 2018 exhibit markedly greater amplitude than the remainder of the series. The propagation of extreme outliers through gauge processing caused the inflation of the 3σ threshold used to identify storm surge events. Consequently, the flagged storm surge events from the Mumbles tide gauge are likely residual errors from ineffective gauge processing and tidal prediction.

An alternative approach to tidal prediction was therefore implemented using RTide, a machine-learning framework based on the tidal response method[21,22]. Unlike HA methods that represent tides as a combination of periodic constituents, RTide learns the relationship between astronomical tidal forcing and sea level variability, better accounting for non-stationary behavior and nonlinear interactions between tides and external forcing. This is advantageous for storm surge analyses because conventional HA methods assume a stationary tidal signal and may not account for non-tidal forcing, which can complicate the distinction of tides from storm-driven sea level fluctuation[21]. Furthermore, the RTide model does not need the entire sea level series from a tide gauge for training. Instead, a clean subset of the series can be used to train the model, which can then compute a predicted tide for the full record. Applying RTide to the Mumbles case therefore required inverting the order of the tide gauge preprocessing steps.

For the Mumbles case, a six-year subset of raw tide gauge data from 2000 to 2006 was used to train the RTide model. The trained model was then applied over the full 2002-2020 time series to predict the tide and compute the surge. Outliers were subsequently removed from the surge series using a 3σ criterion. Outlier removal directly from the surge series should be performed cautiously, as it may inadvertently discard genuine extreme events. Its suitability should therefore be assessed for each gauge. For the Mumbles gauge, however, the secondary outlier removal only eliminated values exceeding approximately 5 m, which are unrealistic in the context of the full surge time series. The resulting RTide-derived surge is shown in red in Figure 6a.

The storm surge identification and validation procedure was then performed using the new surge series. The new storm surge results are presented in Figure 6b in red, together with the corresponding AX altimetry (blue) and ADB altimetry (black). The number of captured storm surges decreased from 13 to two, while agreement between the tide gauge and altimetry improved substantially. For the 2002 event, the difference between the tide gauge and AX altimetry was just 0.008 m. There was no available ADB altimetry data on this day for comparison. For the 2004 event, the differences were approximately 0.2 m for AX and 0.4 m for ADB. While gauge-altimetry differences remain, they are considerably smaller than the multi-meter discrepancies observed during the original validation procedure.

The Mumbles case study emphasizes the challenges of applying a single processing framework across a global network of gauges. Although standardized processing facilitates controlled comparisons between locations, it does not consider the differences in local tidal dynamics, coastal geometry and data quality. Future work could therefore investigate location-specific processing approaches that account for these differences, as well as criteria for excluding gauges where local conditions, including land-sheltering, limit their suitability for altimetry validation. This case study, however, does establish RTide as universally preferable to conventional harmonic analysis (HA) for storm surge detection. HA remained suitable for most gauges

in this study, whereas RTide provides a viable alternative at locations where complex tidal dynamics can compromise the derived surge series.

Extending the findings of this case study to the broader validation results suggests that tide gauge processing errors likely contribute to the largest discrepancies observed in Figure 3, rather than poor altimetry performance. Accordingly, the 24 gauges in the AX dataset and 30 in the ADB dataset for which most gauge-altimetry differences fall outside the 5th-95th percentile range are excluded from the remainder of the analysis to reduce the influence of unreliable storm surge estimates on the assessment of altimetry performance.

Evaluation of Altimetry Storm Surge Detection Against Gauge-Defined Thresholds

Figure 7 compares the storm surge sea levels measured by AX and ADB with the corresponding 3σ thresholds derived from the matched tide gauges. Ratios above 1 indicate that the altimetry-derived surge exceeds the gauge-defined threshold, representing a successful capture of a storm surge. AX exceeds the threshold in 52.42% of events, compared with 45.42% for ADB.

Although the overall distributions indicate comparable variability for AX and ADB with the tide gauge, their individual ratios reveal substantial differences in performance. Many ratios cluster around 1, indicating that the AX or ADB-derived surges are close to the gauge-defined threshold. In contrast, a considerable number fall far below or above. This suggests that the ability of altimetry to capture storm surge sea levels depends on the conditions under which the observations are acquired. These discrepancies may reflect several factors, including physical differences between individual storm events, coastal configuration, and the spatial separation between measurement points. Altimetry tracks were matched to tide gauges using a 50 km search radius around the gauge. Within this distance, coastal morphology and hydrodynamic conditions can widely vary. Bays, barrier islands, and other coastal features can alter how a storm surge is expressed locally. This presents a fundamental challenge for point-based validation, as storm surges are spatially evolving phenomena and measurements at different locations may capture distinct expressions of the same surge. The following section examines the influence of the distance between satellite measurements and tide gauges, while future work could further investigate the underlying forcing effects and physical processes contributing to gauge-altimetry disagreement.

Closing the Distance with GTSM

To investigate the influence of spatial mismatch, GTSM is introduced as an additional reference, allowing storm surge estimates to be compared with smaller spatial offsets due to the higher resolution of the model. The following analysis focuses on the AX dataset, which provides a larger number of storm surge observations than ADB for validation for the tide gauge and model.

Comparing storm surge estimates from GTSM at the nearest altimetry point (GTSM@AX) and at the tide gauge location (GTSM@TG) reveals a strong correlation of 0.97, indicating that the model produces highly consistent estimates at the two locations (Figure 8a). This consistency is plausible given the close proximity of the two locations and the relatively coarse spatial resolution of the meteorological forcing parameters, which can limit the variability in the simulated surge within small distances[14]. Figure 8b shows GTSM (GTSM@AX) and AX altimetry also capturing very similar storm surge signals, as indicated by their strong correlation (0.91). Although high agreement between GTSM and altimetry does not independently establish the accuracy of either dataset, it provides additional evidence that the two approaches consistently represent the observed sea level variability. Comparing AX altimetry with tide gauge observations in Figure 8c), the correlation decreases to 0.71, largely due to outliers where the tide gauge records extreme sea levels while the corresponding altimetry values remain close to zero. Comparing the tide gauge with its nearest GTSM coincident sea level estimate provides further insight into the cause of these discrepancies. In (Figure 8d), similar outliers are evident, suggesting that these extreme values may not represent actual storm surge signals misrepresented by the altimetry. Instead, the consistency between GTSM and altimetry points again towards errors in the tide gauge processing.

Figure 9a compares event-based differences between AX altimetry and the nearest GTSM estimate, tide gauge observations and AX altimetry, and tide gauge observations and the nearest GTSM estimate. Although most differences cluster near zero, both comparisons involving tide gauges (red and light blue) include a number of large discrepancies. In contrast, differences between AX altimetry and GTSM (dark blue) are generally smaller, with a mean of 0.141 m, compared with 0.214 m for the tide gauge-GTSM comparison and 0.210 m for the tide gauge-altimetry comparison.

Figure 9b, however, contradicts the idea that spatial separation may be a driving the primary factor driving these large differences. The distances between comparison points show no clear relationship with the magnitude of the differences. Large gauge-altimetry discrepancies can occur at distances of up to 50 km, but similarly large separations are also observed when the differences are minimal. Likewise, large distances do not necessarily correspond to large differences between the tide gauge, altimetry, and GTSM.

Data and Methodology

Tide Gauge Data and Preprocessing

Global sea level observations from 6,682 tide gauges were obtained from the GESLA-4.1 dataset[23]. These records provide the reference data used to identify days on which storm surge events occurred. Before identifying storm surge events, the data were quality-controlled to minimize the propagation of outliers and discontinuities from the raw series into the predicted tide and the resulting surge using the methodology implemented in Calafat and Marcos (2020)[24]. First, missing data from the raw sea level records were removed. Sudden changes in the mean of the records, which can arise from adjustments to reference levels or instrumental issues, were identified using a change-point detection method[25]. The record was then divided into segments with similar datum values, and the mean of each segment was subtracted to center all segments around zero. Outliers in the series were then identified using a moving-median filter, where individual data points were evaluated relative to the local median. Observations that exhibited significant deviation from their immediate surroundings were flagged as anomalous and removed.

The astronomical tide was estimated from the corrected sea level using UTide[26]. UTide is a HA method that represents the periodicity in sea level with derived tidal constituents. These tidal constituents were subsequently used to reconstruct the predicted astronomical tide across the entire sea level record. The analysis was performed independently for each year, combining the resulting annual predictions to produce a continuous tidal signal across the time series. The reconstructed tide was then compared with the corrected sea level record to identify and correct potential phase discrepancies. Finally, the predicted tide was linearly interpolated onto the original observation times, and the storm surge was calculated as:

$$SS(t) = SL_{\text{processed}}(t) - T_{\text{predicted}}(t),$$

where $SS(t)$ is the surge residual, $SL_{\text{corrected}}(t)$ is the corrected sea level series, and $T_{\text{predicted}}(t)$ is the reconstructed tide. The residual series represents sea level variability not caused by tidal variation. The resulting storm surge time series, together with the intermediate preprocessing steps, is presented for one example tide gauge in Supplementary Figure 7.

Extreme sea level events were identified in the resulting surge series using a 3σ threshold. The mean and standard deviation of the surge for each tide gauge were calculated, and individual observations exceeding three standard deviations above the mean were classified as extreme. Unique calendar days with at least one extreme observation were then defined as storm surge days. Applying this methodology to the valid tide gauge records resulted in 269,237 storm surge days flagged across all valid locations within the study period.

Coastal Altimetry Data

Two coastal altimetry datasets were used in this study. The first was the along-track, 10-day, 20-Hz coastal altimetry dataset developed as part of the ESA Sea Level CCI project. The product combines the ALES retracker[16] with the X-TRACK processing system[27] and is based on the original 20-Hz along-track Jason-1, Jason-2, and Jason-3 altimetry observations. The data have a temporal resolution of 9.915-day repeat cycles and a spatial resolution of 300 m[27].

Depicted as the red regions in Figure 10, the AX coastal altimetry data obtained for this study are distributed across six global regions: (1) the Northeast Pacific, (2) the Northwest Atlantic, (3) the Northeast Atlantic, (4) the Southwest Indian Ocean, (5) the Northern Indian Ocean, and (6) the Indo-Pacific regions.

To test the robustness of the findings, a second coastal altimetry dataset was obtained from the DGFI-TUM Open Altimeter Database (ADB)[18]. The 20-Hz SLA of the ALES product version number 56 is used from ADB and is freely available online. Although ADB (blue region, Figure 10) provides global coverage from several altimetry missions, only Jason-1, Jason-2, and Jason-3 data corresponding to the same ground tracks and cycles as the AX dataset were considered for comparative purposes. The altimetry data used in this study span the period from 2002 to 2020.

Altimetry-Derived Sea Level Variables

SLA and DAC data were obtained from two satellite altimetry products to characterize coastal sea level variability. SLA is represented by the deviation of the measured sea surface height (SSH) from a reference mean sea surface (MSS). Following Lobeto et al. (2018)[28], sea-surface height (SSH) is calculated relative to the reference ellipsoid from the satellite altitude (H) and the satellite-to-surface range (R). In this study, R is obtained using the ALES-retracked range. Corrections are applied to this observed range (R_{obs}) to account for errors introduced by atmospheric propagation delays and radar measurement biases. These corrections include the dry tropospheric correction (DTR), wet tropospheric correction (WTR), ionospheric correction (IONO), and sea-state bias correction (SSB). SSH can then be represented as:

$$\text{SSH} = H - (R_{\text{obs}} + \text{DTR} + \text{WTR} + \text{IONO} + \text{SSB})$$

Additional adjustments are then applied alongside range corrections to account for variations in the sea surface caused by geophysical effects. These include the tidal correction (TIDES), and the DAC. After applying the relevant corrections, SLA is obtained by subtracting the MSS from SSH. In this study, the MSS was derived from the mean of the available satellite tracks. The resulting SLA is calculated as follows:

$$\mathrm{SLA} = H - R_{\mathrm{obs}} - DTR - WTR - IONO - SSB - \mathrm{TIDES} - \mathrm{DAC} - \mathrm{MSS}.$$

The DAC is a modeled quantity that accounts for sea level variations induced by atmospheric pressure and wind forcing. Described by Carrere and Lyard (2003)[29], it consists of a low-frequency component computed with the classical inverse barometer approximation, which describes how sea level responds to variations in atmospheric pressure, and of a high-frequency component obtained from the MOG2D hydrodynamic model, which estimates the ocean response to high-frequency wind forcing[29].

When investigating storm surges using altimetry data, the DAC must be added back to the SLA because it accounts for sea level variability driven by atmospheric pressure and wind, two key drivers of storm surges. Adding the DAC to the SLA (SLA+DAC) represents sea level variability, including the modeled atmospheric contribution restored and excluding the predicted astronomical tide, providing a more complete representation of the sea level response during storm events[28].

Spatiotemporal Colocation

To enable validation of altimetry-derived sea level observations against tide gauge measurements, the AX and ADB altimetry tracks were spatially colocated with valid gauge locations. Few satellite ground tracks pass directly over tide gauges, necessitating a search radius to identify gauge-altimetry matches. A 50 km radius was adopted, consistent with previous work: Vega-Gimenez et al. (2025)[30] selected a 50 km search radius following a sensitivity analysis, which identified a stable minimum in RMSD between 40 and 60 km. Any altimetry track segment located within 50 km of a tide gauge was matched to that gauge. This threshold provides a consistent basis for global comparisons while retaining a sufficient number of matched observations. However, geographic proximity does not necessarily imply that the two observing systems sample the same sea level response. As discussed in detail in Closing the Distance with GTSM in the Results and Discussion, reducing the search radius may not guarantee better agreement, particularly in a global analysis where coastal configurations differ substantially and physical conditions can vary greatly within small distances.

The resulting match cases revealed two distinct track approach orientations, parallel and perpendicular, as well as a range of complex coastal configurations, including regions with barrier islands and other land-shielding features (Figure 11).

Finally, all instances in which a satellite passed within the 50 km search radius while the tide gauge recorded sea levels exceeding the respective 3σ threshold were defined as storm surges.

Filtering the High-frequency Altimetry Data

While AX and ADB products provide the spatial resolution needed to capture short-term coastal dynamics, high-rate data contain substantial noise that may not reflect true sea level fluctuations. This is particularly pronounced the closer the data are to the coast, where large positive and negative outliers in sea level anomaly can obscure the storm surge signal. These outliers can arise from signal contamination (land or patches of very calm water within the satellite footprint) and complex coastal dynamics[13,31]. Reliable identification of storm surges from the altimetry data, therefore, requires a filtering approach that removes outliers and unrealistic variability while preserving the underlying sea level signal.

To achieve this, a three-stage filtering framework was developed combining outlier detection, smoothing, and regression. Outliers are identified and removed using the Density-Based Spatial Clustering of Applications with Noise (DBSCAN) algorithm[32]. DBSCAN groups individual data points based on the density of neighboring points, allowing observations existing outside of a sufficiently dense cluster to be classified as extremes and removed. The remaining data are then smoothed using a Gaussian filter. Finally, Locally Weighted Scatterplot Smoothing (LOWESS) regression[33] was applied to estimate the underlying sea level signal while preserving larger-scale along-track gradients.

The filtering procedure is controlled by four parameters: the DBSCAN neighborhood radius (ε), the DBSCAN minimum number of observations required to form a cluster (minsamples), the Gaussian kernel width (σ), and the LOWESS smoothing fraction (frac). These parameters were optimized using a representative subset of 100 tide gauge locations that had (1) no gaps in the surge series and (2) at least 5 years of data.

Parameter optimization was performed using 81 parameter combinations ($\varepsilon = 0.04, 0.06, 0.08$, minsamples $= 4, 6, 8$, $\sigma = 0.5, 1.0, 1.5$, and frac $= 0.10, 0.15, 0.20$). For each combination, the filter was applied to the segment altimetry data colocated with each tide gauge. The SLA+DAC observation nearest to the coast was then extracted for each available satellite overpass, not only storm surge days, and compared with the coincident tide gauge measurement.

An example of this process for one tide gauge is shown in Figure 12. Panel (a) shows the paired AX and tide gauge time series using the optimized parameter set. Light blue indicates the AX SLA+DAC points nearest to the coast from the unfiltered

along-track data, while dark blue indicates the corresponding observations after filtering. Tide gauge observations recorded at the same time as the altimetry measurements are shown in red. The unfiltered AX data contain numerous outliers, whereas many of these are eliminated in the filtered observations that more closely follow the tide gauge measurements. Panel (b) shows similar results for ADB, with unfiltered observations shown in gray, filtered observations in black, and the tide gauge data in red.

The correlation coefficient between the filtered altimetry and tide gauge time series was calculated for each gauge location, and the parameter combination yielding the highest correlation was selected as optimal. The resulting optimal parameter set was $\varepsilon = 0.04$, minsamples $= 8$, $\sigma = 1.5$, and frac $= 0.20$. These values were applied to both the AX and ADB datasets. Across all tested gauge locations, the mean correlation was 0.5251 for AX and 0.5260 for ADB, with maximum correlations of 0.9107 and 0.8628, respectively.

Comparing Nearest-to-coast and Nearest-to-gauge

To validate the satellite's performance against the tide gauges and best capture the coastal storm surge signal, there were two options available for the comparative altimetry data point: the nearest-to-gauge (NTG) point and the nearest-to-coast (NTC) point. The NTC point was preferred as it ensured a sea level signal more reflective of coastal conditions. The NTG point was also considered as it may be more comparable with the tide gauge. The NTG point was frequently located outside of the coastal zone in more open waters, particularly when the satellite ground track approached the shore with a more parallel orientation. Therefore, the NTC and NTG points were directly compared to verify that choosing the NTC point over the NTG point introduced no significant error. Figure 13 depicts the absolute difference between NTC and NTG SLA+DAC points for all storm surges captured at all locations for both the AX and ADB datasets, together with the relative frequencies of their mean differences. Average absolute differences of approximately 3 cm were computed for both datasets, with 80% of the data falling between 0 and 5 cm.

Because the NTC and NTG points are both located within the 50 km search radius of the tide gauge and the majority of events show differences of less than 5 cm between the two points, the NTC point was considered sufficiently representative for the subsequent analysis. This also allowed for the distance-to-coast variable associated with each coastal altimetry product to be used in the analysis.

Impacts of Filtering Method

An example demonstrating the methods and filtering is presented for the Maasvlakte-Amaliahaven, NL altimetry-gauge match case (Figure 14b), displaying the SLA+DAC vs. latitude on 01 April 2017 (Figure 14a). For both the AX and ADB datasets, the unfiltered altimetry data (pink and grey) clearly demonstrate the variability and extreme outliers that are successfully eliminated in the filtered signals (red and black). Focusing on the NTC point, the unfiltered AX SLA+DAC data contains a severe negative outlier, whereas the filtered signal records a value of 0.889 m. For validation, Figure 14c presents the tide gauge time series on the storm surge date, where the red line indicates a gauge-observed sea level of 0.902 m at the time of the altimetry pass. The close agreement between the tide gauge measurement and the filtered AX SLA+DAC NTC observation demonstrates that filtering is essential for capturing peak storm surge events; without it, the storm surge signal may be obscured by high-frequency noise and missed.

GTSM Hydrodynamic Model

While tide gauges can provide accurate ground truth, they represent a point measurement and therefore the distance to the altimetry track may be an issue when validating the altimeter measurements. Hydrodynamic models can therefore be used to evaluate the impact of the distance between tide gauges and altimetry, since they provide data on regularly spaced coastal segments or grids. Surge reanalysis data were obtained from the GTSM, version 3.0. GTSM uses the Delft3D Flexible Mesh (Delft3D-FM) modeling system and an unstructured computational grid, allowing high spatial resolution of simulated data in shallow coastal regions[14]. The model provides 10-minute, hourly, and daily maximum surge estimates at spatial resolutions of approximately 2.5 km globally and 1.25 km along the European coast, with hourly estimates used in this study.

The GTSM total water level comprises the tidal elevation, storm surge, and changes in annual mean sea level, and is referenced to mean sea level over the 1986–2005 period. The tidal elevation is obtained from the simulation forced only by celestial tide-generating forces, without meteorological forcing from wind or atmospheric pressure, and therefore represents the pure astronomical tide. The GTSM storm surge is then calculated as the residual between the total water level and the tidal elevation, with changes in annual mean sea level accounted for separately. Detailed information about the variables can be found on the Climate Data Store download portal. Validation findings from Aleksandrova et al. (2026)[34] demonstrate strong model performance compared with tide gauges. Evaluation of individual storms confirms that the model accurately captures the timing of extreme events, but peak magnitudes are occasionally underestimated due to the resolution of forcing parameters[34].

To validate the altimetry data against GTSM, modeled surge values corresponding to the date and hour of each altimetry observation were extracted from the nearest GTSM grid point and compared with the NTC observation and tide gauge. The

GTSM data were used as an independent reference, and no altimetry was assimilated into the model. Further information on GTSM is available through the public GTSM wiki.

Comparability of Sea Level Estimates

GTSM-derived surge reanalysis, tide gauge-derived surge, and the altimetry-derived SLA+DAC provide complementary representations of non-tidal sea level variability during extreme events. Although the data are derived from different systems, they each capture sea level variations influenced by atmospheric forcing and remove the astronomical tide, allowing their representation of extreme sea level events to be comparable.

Their comparability, however, does not imply that coincident estimates are identical. Tide gauges measure sea level at a fixed point, satellite altimetry samples along discrete ground tracks, and GTSM represents sea level variability on a spatial grid. These differences in spatial and temporal resolution are particularly important when observing extreme events, which can evolve rapidly and produce very strong sea level gradients. The resolution of meteorological inputs in gridded model estimates, together with the discrete sampling of satellite altimetry, may dampen or fail to capture the full magnitude of extreme events compared with a reference tide gauge. Additionally, differences in vertical reference systems must also be considered, as inconsistent reference levels can introduce additional discrepancies. Standardizing these references in future validation work would improve the consistency of validation data with altimetry data.

Conclusion

Despite limitations in spatial coverage and revisit frequency, high-rate coastal altimetry offers a valuable means of observing storm surges on a global scale. This study demonstrates that high-rate altimetry data can not only detect storm surges with strong gauge-altimetry agreement but can also provide a means of systematically validating storm surge model predictions in areas where tide gauges are unavailable. To reliably extract the storm surge signal for these applications, however, the data must be filtered to remove outliers and small-scale variability arising from interactions between the radar signal and the coastal environment. To achieve this, a filtering framework combining DBSCAN outlier detection, Gaussian smoothing, and LOWESS regression was developed to extract the underlying sea level signal.

The analysis identified 1,629 storm surges across 540 tide gauge locations using AX and 1,396 captures across 505 locations using ADB. Both altimetry datasets generally underestimate storm surge sea levels relative to tide gauge observations, while capturing sea levels that exceeded the gauge-defined extreme event threshold in approximately half of the cases. Investigating tide gauges with significant gauge-altimetry disagreement revealed that the large differences may not necessarily be attributable to a failure of altimetry to capture storm surge signals, but rather errors introduced in the tide gauge processing. Outliers and segments of unreliable data in raw tide gauge records can propagate through tidal prediction and into the derived surge signal, leading to the misidentification of extreme events. This was demonstrated by the Mumbles tide gauge case study, where applying an alternative processing approach substantially improved gauge-altimetry agreement. Although the processing methodology of Calafat and Marcos (2020)[24] performed well across the majority of locations, the Mumbles case highlights the importance of fine-tuning the tide gauge processing for specific locations, where local physics may limit the effectiveness of conventional HA methods for tidal prediction.

Finally, comparison with GTSM provided further insight into the influence of spatial distance on gauge-altimetry agreement. GTSM estimates showed strong agreement between the altimetry and tide gauge locations, as well as with AX altimetry. Consequently, GTSM exhibited similarly weaker agreement with tide gauge measurements as altimetry, regardless of spatial separation. Even when GTSM estimates were compared at locations with smaller spatial offsets than those between tide gauges and altimetry observations, discrepancies persisted in both the GTSM-gauge and gauge-altimetry comparisons, suggesting that spatial separation alone is insufficient to explain the observed discrepancies. The similarities between storm surge estimates from altimetry and GTSM suggest that both systems may be limited in their ability to capture local processes that influence extreme coastal sea levels. This highlights the need for more research into the physical processes governing storm surge development in coastal environments, including the roles of local wind forcing, wave setup, coastal morphology, and other site-specific factors. Accounting for these processes will be crucial for improving both the interpretation of coastal altimetry observations as well as the representation of extreme sea levels in storm surge models.

Expanding the analysis to additional satellite altimetry missions would further improve the temporal and spatial sampling of coastal sea level and increase the number of storm surge events that can be observed from space. The Surface Water and Ocean Topography (SWOT) mission offers a particularly promising opportunity to extend this work by providing spatially distributed observations of coastal sea level variability at substantially higher spatial resolution than conventional along-track altimetry. This capability could enable storm surge to be examined not only as a localized sea level anomaly, but as a spatially evolving phenomenon, providing new insight into how the coastal environment and storm characteristics interact to shape its magnitude and spatial footprint[30]. Together, these developments offer a pathway toward using satellite observations not simply to detect

storm surge events, but also to observe storm surges in areas lacking in-situ data and examine how local coastal characteristics shape the physical expression of the surge.

Acknowledgements

The authors are grateful to the Sea Level CCI Consortium for providing, upon request, the along-track 10-day 20 Hz coastal altimetry dataset used in this study.

We thank Marta Marcos for the valuable discussions on tide gauges and for sharing her expertise in tide gauge data correction and processing. We thank Thomas Monahan for his guidance on using RTide and insights into complex tide dynamics. We are also grateful to Natalia Aleksandrova for her contributions to our understanding of hydrodynamic modeling of storm surges.

Funding

J.P.J. acknowledges funding from the European Space Agency's Climate Change Initiative (CCI) under the Climate Space: Climate Change and Cities Activity, Contract No. 4000148747/25/I/LR. Additional information about the project can be found on the project website.

Data and Code Availability

The working code and a sample of data used in this analysis are available at https://github.com/jemmajohns0n/stormsurge.git. The DGFI-TUM Open Altimeter Database (ADB) is publicly accessible at: https://openadb.dgfi.tum.de/en/.

Author Contributions

J.P.J. developed and implemented the analytical methodology, conducted the data processing analysis, produced the figures, interpreted the results, and wrote the manuscript. M.P. and M.G.H.D. established the research direction and conceptual foundation of the study, providing scientific guidance throughout its development. M.G.H.D. and M.P. provided ongoing supervision, feedback, and guidance on the research approach and findings. B.B. contributed expertise and guidance on hydrodynamic modeling, while C.S. provided guidance on the DGFI-TUM Open Altimeter Database (ADB). All authors reviewed and edited the manuscript.

Competing interests

The authors declare no competing interests.

References

1. Barroso, A., Wahl, T., Enriquez, A., Morim, J. & Dangendorf, S. Changes in the seasonal cycle of storm surge along the global coastline. *Journal of Geophysical Research: Oceans* (2025). URL https://doi.org/10.1029/2024JC022187.

2. Vousdoukas, M. I., Voukouvalas, E., Annunziato, A., Giardino, A. & Feyen, L. Projections of extreme storm surge levels along europe. *Climate Dynamics* **47**, 3171–3190 (2016). URL https://doi.org/10.1007/s00382-016-3019-5.

3. Koh, Z. Y. *et al.* Tide–surge interaction observed at singapore and the east coast of peninsular malaysia using a semi-empirical model. *Ocean Science* **20**, 1495–1511 (2024). URL https://doi.org/10.5194/os-20-1495-2024.

4. Rappaport, E. N. Fatalities in the united states from atlantic tropical cyclones: New data and interpretation. *Bulletin of the American Meteorological Society* **95**, 341–346 (2014). URL https://doi.org/10.1175/BAMS-D-12-00074.1.

5. Needham, H. F., Keim, B. D. & Sathiaraj, D. A review of tropical cyclone-generated storm surges: Global data sources, observations, and impacts. *Reviews of Geophysics* **53**, 545–591 (2015). URL https://doi.org/10.1002/2014RG000477.

6. Barros, J. L., Tavares, A. O., Santos, P. P. & Freire, P. Enhancing a coastal territorial vulnerability index: Anticipating the impacts of coastal flooding with a local scale approach. *Coastal Management* **50**, 442–468 (2022). URL https://doi.org/10.1080/08920753.2022.2107858.

7. Ma, P. & Li, G. Comparison and analysis of detection methods for typhoon-storm surges based on tide-gauge data—taking coasts of china as examples. *International Journal of Environmental Research and Public Health* **20**, 3253 (2023). URL https://doi.org/10.3390/ijerph20043253.

8. Antony, C., Testut, L. & Unnikrishnan, A. Observing storm surges in the bay of bengal from satellite altimetry. *Estuarine, Coastal and Shelf Science* **151**, 131–140 (2014). URL https://doi.org/10.1016/j.ecss.2014.09.012.

9. Han, G., Ma, Z., Chen, D., deYoung, B. & Chen, N. Observing storm surges from space: Hurricane igor off newfoundland. *Scientific Reports* **2** (2012). URL https://doi.org/10.1038/srep01010.

10. Chen, N., Han, G., Yang, J. & Chen, D. Hurricane sandy storm surges observed by hy-2a satellite altimetry and tide gauges. *JGR Oceans* **119**, 4542–4548 (2014). URL https://doi.org/10.1002/2013JC009782.

11. Harwood, P. eSurge final report. Technical Report, CGI (2015). URL https://due.esrin.esa.int/files/20150310050027.pdf.

12. Hart-Davis, M. G. *et al.* Tide of the time: Global tidal characteristics observed from in-situ measurements. *Ocean Science* **22**, 1681–1709 (2026). URL https://doi.org/10.5194/os-22-1681-2026.

13. Cipollini, P., Calafat, F. M., Jevrejeva, S., Melet, A. & Prandi, P. Monitoring sea level in the coastal zone with satellite altimetry and tide gauges. *Surveys in Geophysics* **38**, 33–57 (2017). URL https://doi.org/10.1007/s10712-016-9392-0.

14. Muis, S., Verlaan, M., Winsemius, H. C., Aerts, J. C. J. H. & Ward, P. J. A global reanalysis of storm surges and extreme sea levels. *Nature Communications* **7**, 11969 (2016). URL https://doi.org/10.1038/ncomms11969.

15. Chelton, D., Ries, J. C., Haines, B. J., Fu, L. & Callahan, P. S. in *Chapter 1 satellite altimetry* 69 edn, (eds Fu, L.-L. & Cazenave, A.) *Satellite Altimetry and Earth Sciences* Ch. 1, 1–131 (Academic Press, 2001). URL https://doi.org/10.1016/S0074-6142(01)80146-7.

16. Passaro, M., Cipollini, P., Vignudelli, S., Quartly, G. D. & Snaith, H. M. Ales: A multi-mission adaptive subwaveform retracker for coastal and open ocean altimetry. *Remote Sensing of Environment* **145**, 173–189 (2014). URL https://doi.org/10.1016/j.rse.2014.02.008.

17. Birol, F. *et al.* Coastal applications from nadir altimetry: Example of the x-track regional products. *Advances in Space Research* **59**, 936–953 (2017). URL https://doi.org/10.1016/j.asr.2016.11.005.

18. Schwatke, C. *et al.* OpenADB: DGFI-TUM's open altimeter database. *Geoscience Data Journal* **11**, 573–588 (2024). URL https://doi.org/10.1002/gdj3.233.

19. Lobeto, H. & Menendez, M. Variability assessment of global extreme coastal sea levels using altimetry data. *Remote Sensing* **16**, 1355 (2024). URL https://doi.org/10.3390/rs16081355.

20. Hart-Davis, M. G., Scherer, D., Schwatke, C. *et al.* Observing the tidal pulse of rivers from wide-swath satellite altimetry. *Nature* **652**, 371–378 (2026). URL https://doi.org/10.1038/s41586-026-10287-z.

21. Monahan, T., Tang, T., Roberts, S. & Adcock, T. A. A. RTide: Automating the tidal response method. *Journal of Geophysical Research: Machine Learning and Computation* **2**, e2024JH000525 (2025). URL https://doi.org/10.1029/2024JH000525.

22. Monahan, T., Tang, T., Roberts, S. & Adcock, T. A. Response-based prediction of tidal currents. *Journal of Geophysical Research: Oceans* **130**, e2025JC022758 (2025).

23. Haigh, I. *et al.* Gesla version 4: Further enhancements to the global higher-frequency sea-level dataset. *Earth System Science Data Discussions* (2026). Preprint, in review.

24. Calafat, F. M. & Marcos, M. Probabilistic reanalysis of storm surge extremes in europe. *Proceedings of the National Academy of Sciences of the United States of America* **117**, 1877–1883 (2020). URL https://doi.org/10.1073/pnas.1913049117.

25. Killick, R., Fearnhead, P. & Eckley, I. A. Optimal detection of changepoints with a linear computational cost. *Journal of the American Statistical Association* **107**, 1590–1598 (2012). URL https://doi.org/10.1080/01621459.2012.737745.

26. Codiga, D. L. Unified tidal analysis and prediction using the UTide matlab functions. Technical Report 2011-01, Graduate School of Oceanography, University of Rhode Island, Narragansett, RI (2011). 59 pp.

27. Birol, F. *et al.* The x-track/ales multi-mission processing system: New advances in altimetry towards the coast. *Advances in Space Research* **67**, 2398–2415 (2021). URL https://doi.org/10.1016/j.asr.2021.01.049.

28. Lobeto, H., Menendez, M. & Losada, I. J. Toward a methodology for estimating coastal extreme sea levels from satellite altimetry. *Journal of Geophysical Research: Oceans* **123**, 8284–8298 (2018). URL https://doi.org/10.1029/2018JC014487.

29. Carrère, L. & Lyard, F. Modeling the barotropic response of the global ocean to atmospheric wind and pressure forcing—comparisons with observations. *Geophysical Research Letters* **30**, 1275 (2003). URL https://doi.org/10.1029/2002GL016473.

30. Vega-Gimenez, D., Amores, A., Paris, A. & Pascual, A. Expanding the coastal observation frontier: Swot reveals the spatial footprint of storm surges. *Geophysical Research Letters* **52** (2025). URL https://doi.org/10.1029/2025GL117299.

31. Deng, X. & Featherstrone, W.-E. A coastal retracking system for satellite radar altimeter waveforms: Application to ers-2 around australia. *Journal of Geophysical Research: Oceans* **111** (2006). URL https://doi.org/10.1029/2005JC003039.

32. Ester, M., Kriegel, H.-P., Sander, J. & Xu, X. A density-based algorithm for discovering clusters in large spatial databases with noise. Proceedings of the Second International Conference on Knowledge Discovery and Data Mining (KDD'96) (1996). Conference paper, Portland, Oregon.

33. Cleveland, W. S. Robust locally weighted regression and smoothing scatterplots. *Journal of the American Statistical Association* **74**, 829–836 (1979). URL https://doi.org/10.2307/2286407.

34. Aleksandrova, N., Veenstra, J., & Muis, S. Global dataset of storm surges and extreme sea levels for 1950âĂŞ2024 based on the era5 climate reanalysis. *Earth System Science Data* **18**, 5759–5771 (2026). URL https://doi.org/10.5194/essd-18-5759-2026.

Figures

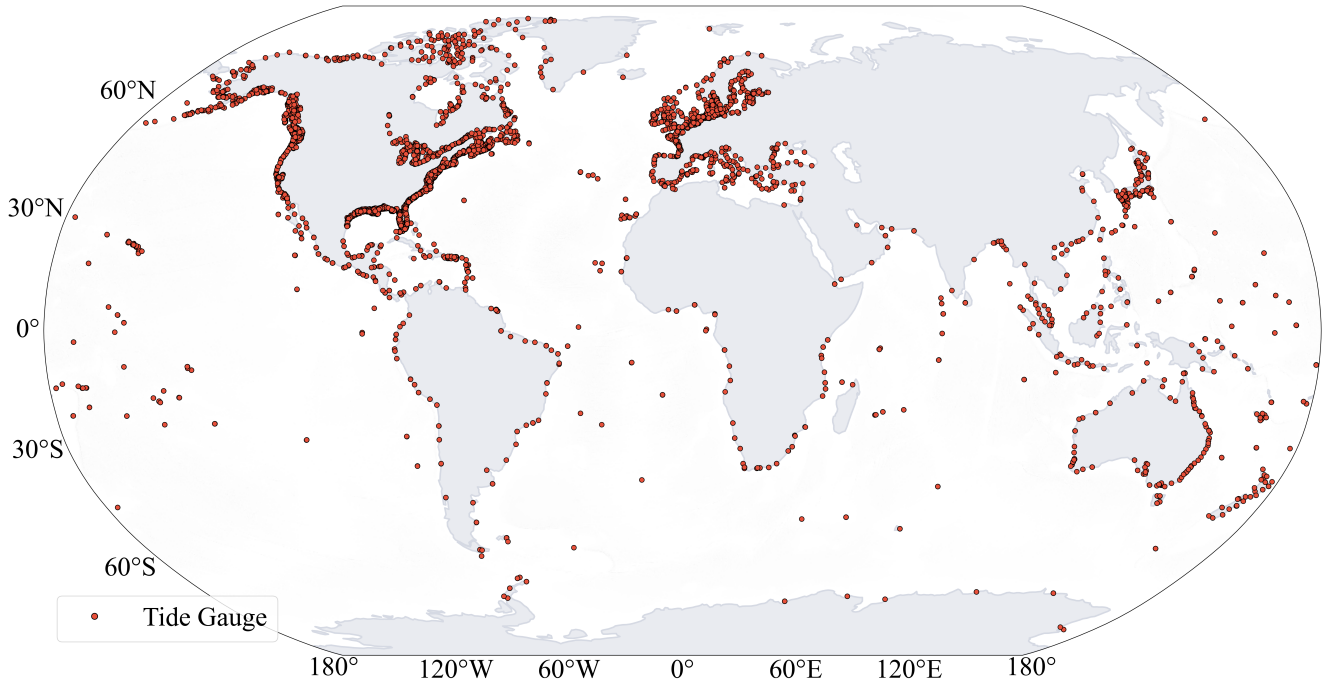


Figure 1. Distribution of publicly available tide gauges observations from GESLA-4.1[23].

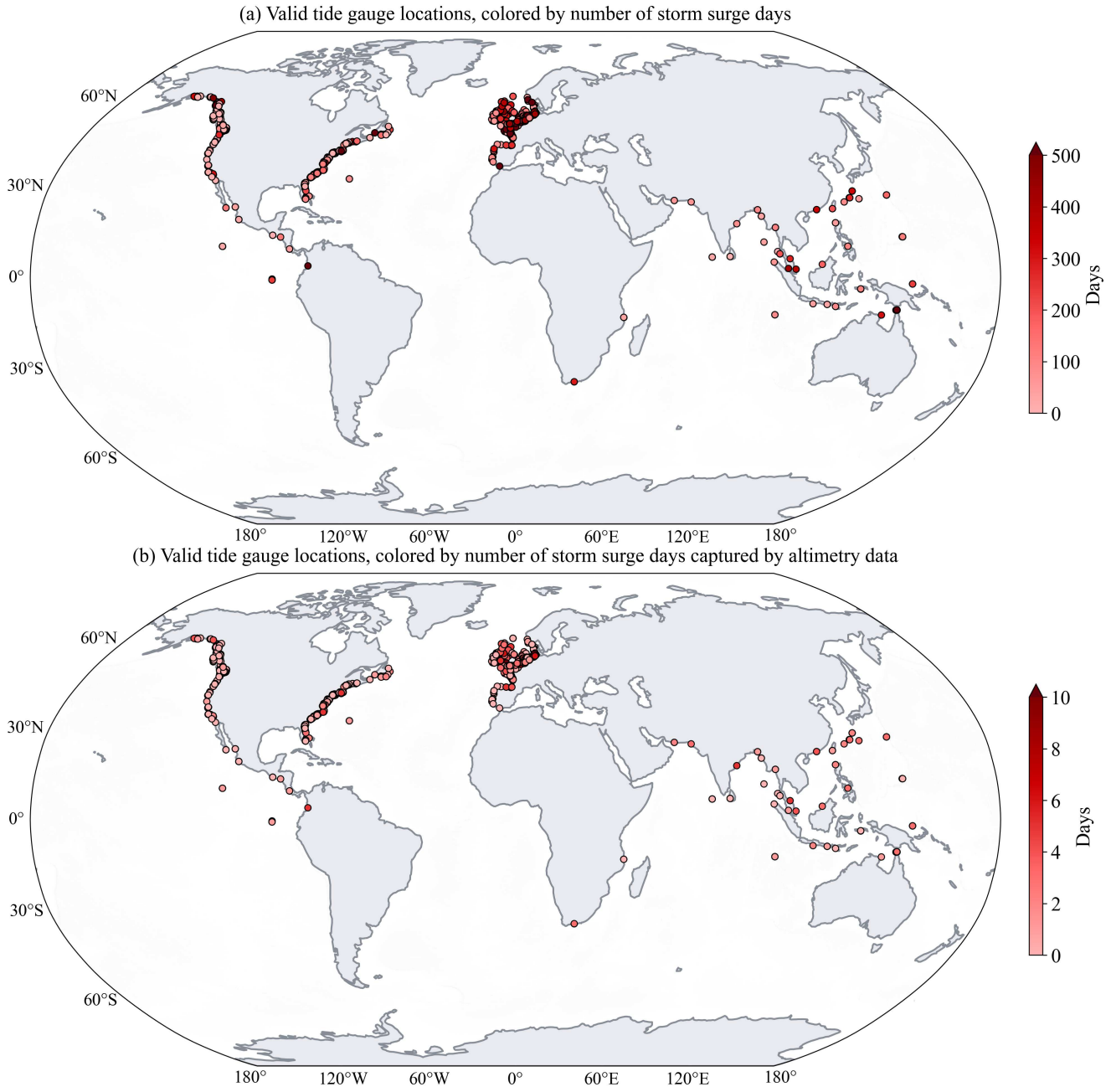


Figure 2. All tide gauge locations matched to an altimetry track, showing (a) the number of unique days with a storm surge and (b) the number of storm surge days observed by an altimetry satellite.

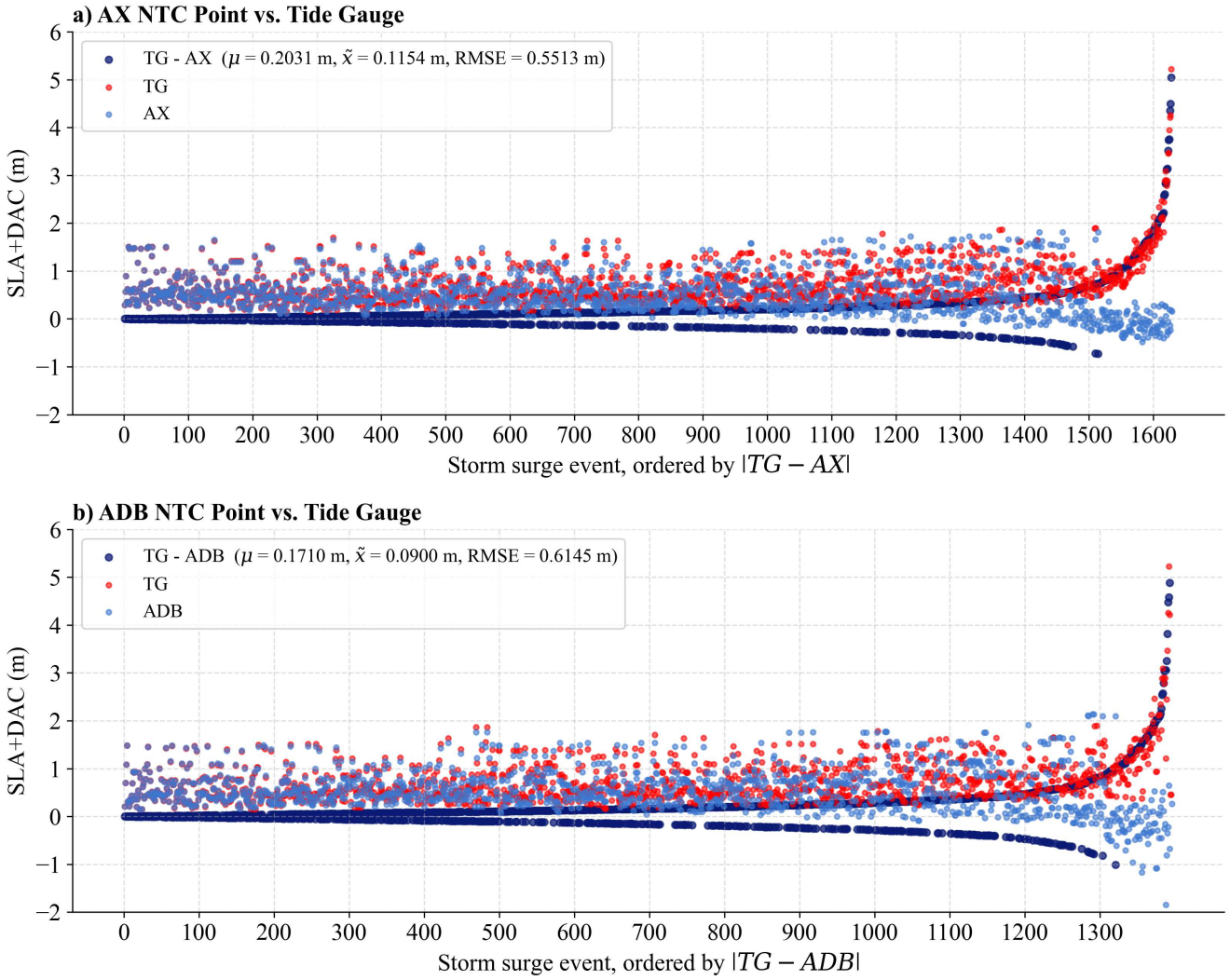


Figure 3. Difference between storm surge measured by the tide gauge and a) AX or b) ADB altimetry.

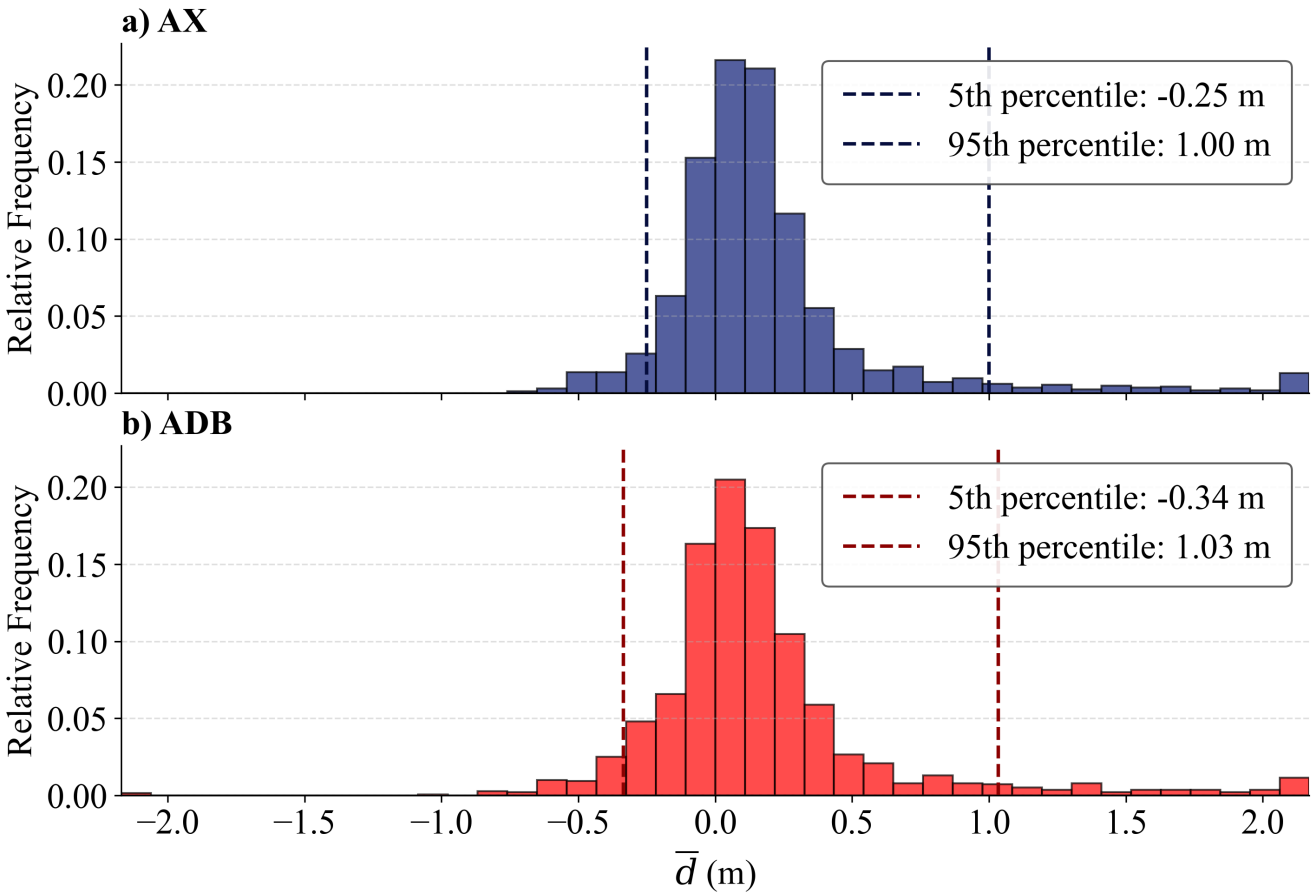


Figure 4. Relative frequency of the tide gauge-altimetry differences.

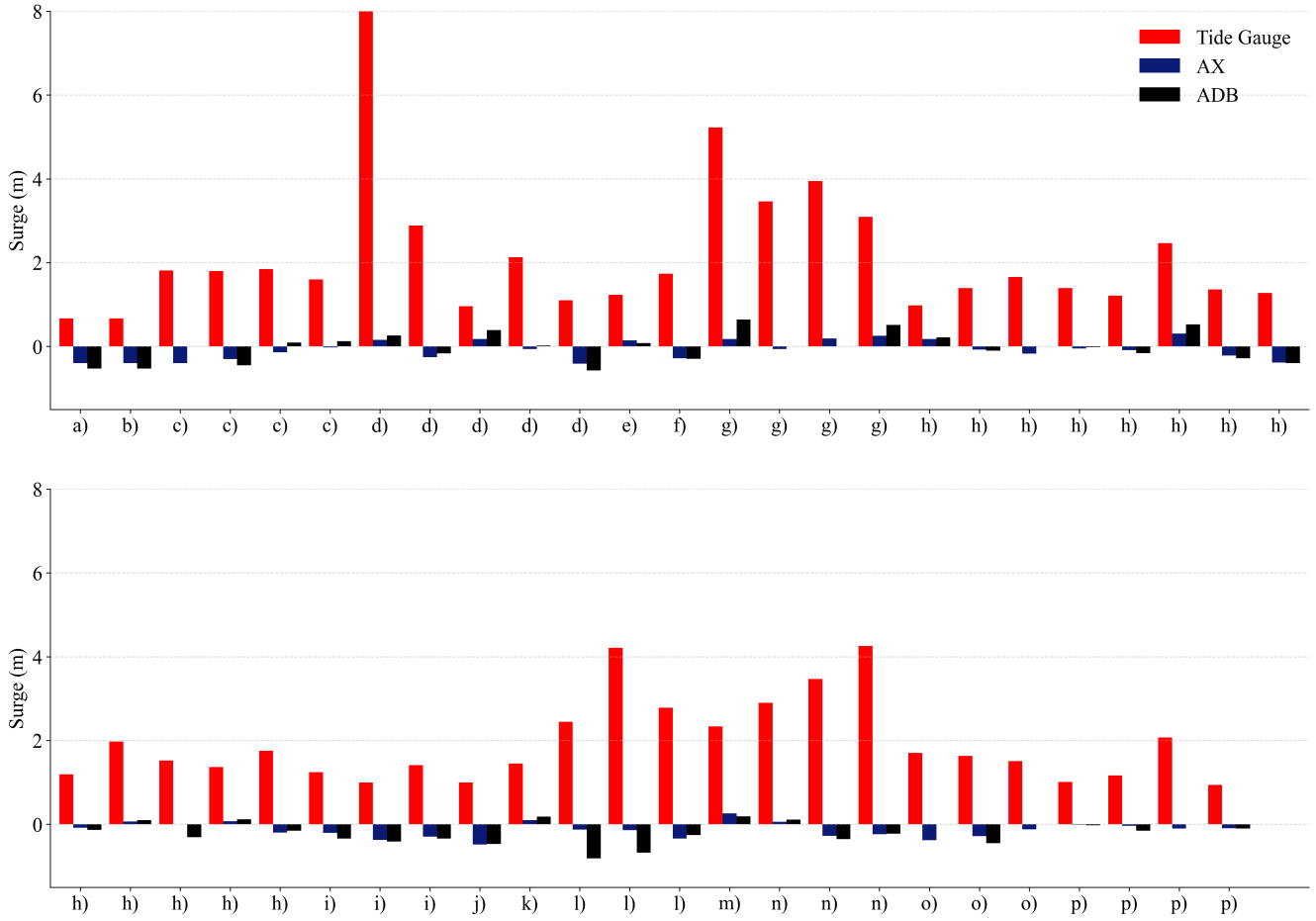


Figure 5. Comparison of tide gauge and satellite altimetry observations during storm surge events at selected tide gauge locations: (a) deal_pier-dlp-gbr-cco (UK); (b) dealpiertg-dea-gbr-cmems (UK); (c) eidersperrwerkbp-9520081-deu-wsv (Germany); (d) holyhead-hol-gbr-cmems (UK); (e) ilfracombe-ilf-gbr-bodc (UK); (f) kinlochbervie-kin-gbr-cmems (UK); (g) leith-lei-gbr-cmems (UK); (h) mumbles-mum-gbr-cmems (UK); (i) nantes_usine_brulee-399-fra-refmar (France); (j) Ppee_dee_river_at_hwy_701_nr_bucksport_sc-2135200-usa-usgs (USA); (k) petten_meetraai_16-pet-nld-rws (the Netherlands); (l) petten_meetraai_17-pet-nld-rws (the Netherlands); (m) petten_meetraai_18-pet-nld-rws (the Netherlands); (n) stmarys-stm-gbr-cmems (UK); (o) tnning-9520070-deu-wsv (Germany); and (p) villefranquetg_05minute-vil-fra-cmems (France).

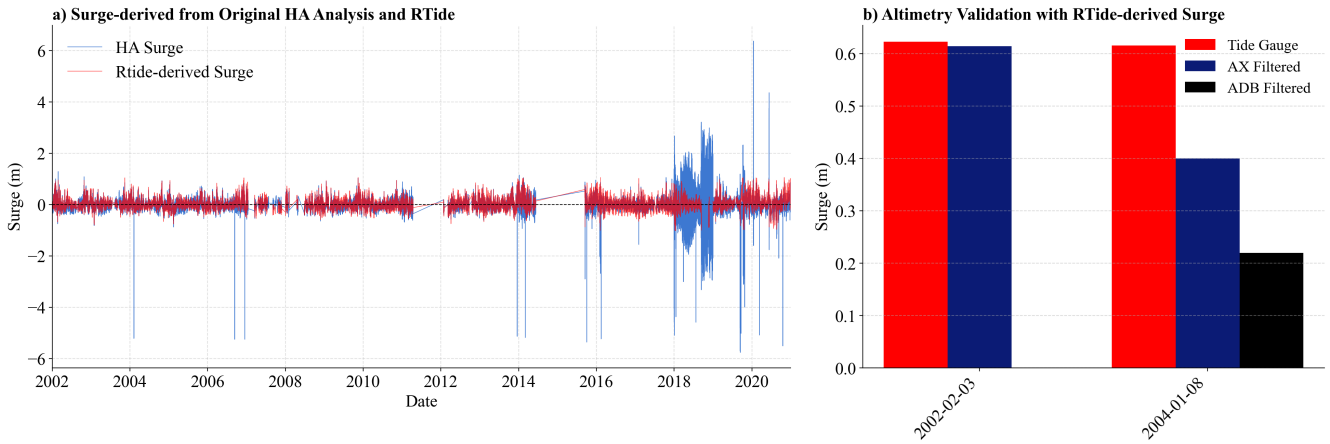


Figure 6. (a) Comparison of the original HA-derived storm surge time series (HA surge) with the RTide-derived storm surge time series. (b) Validation of satellite altimetry storm surge estimates using the RTide-derived tide gauge storm surge as the reference.

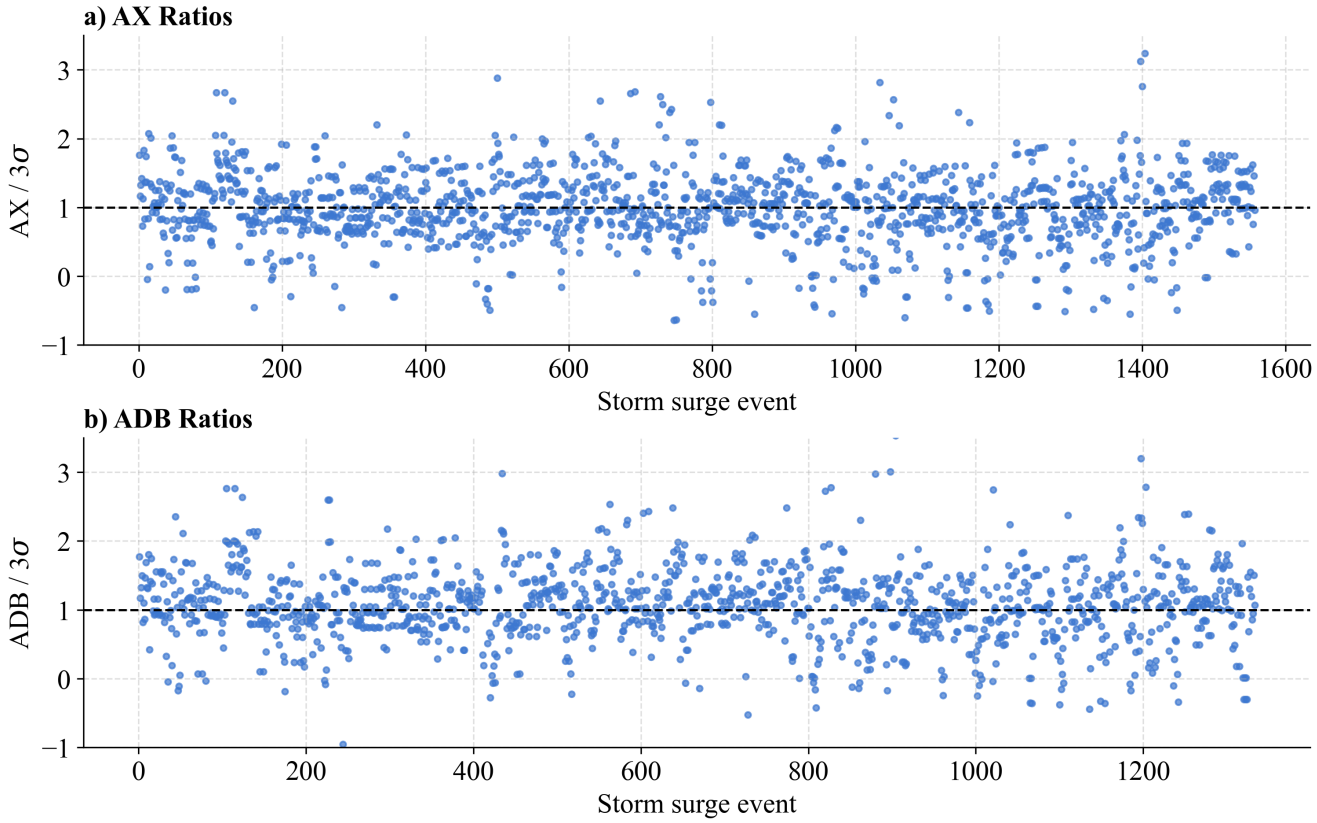


Figure 7. Ratios of altimetry-derived storm surge sea levels to the corresponding 3σ thresholds of the associated tide gauges. AX exceeds the gauge-defined storm surge threshold in 52.42% of events, while ADB exceeds it in 45.42% of events.

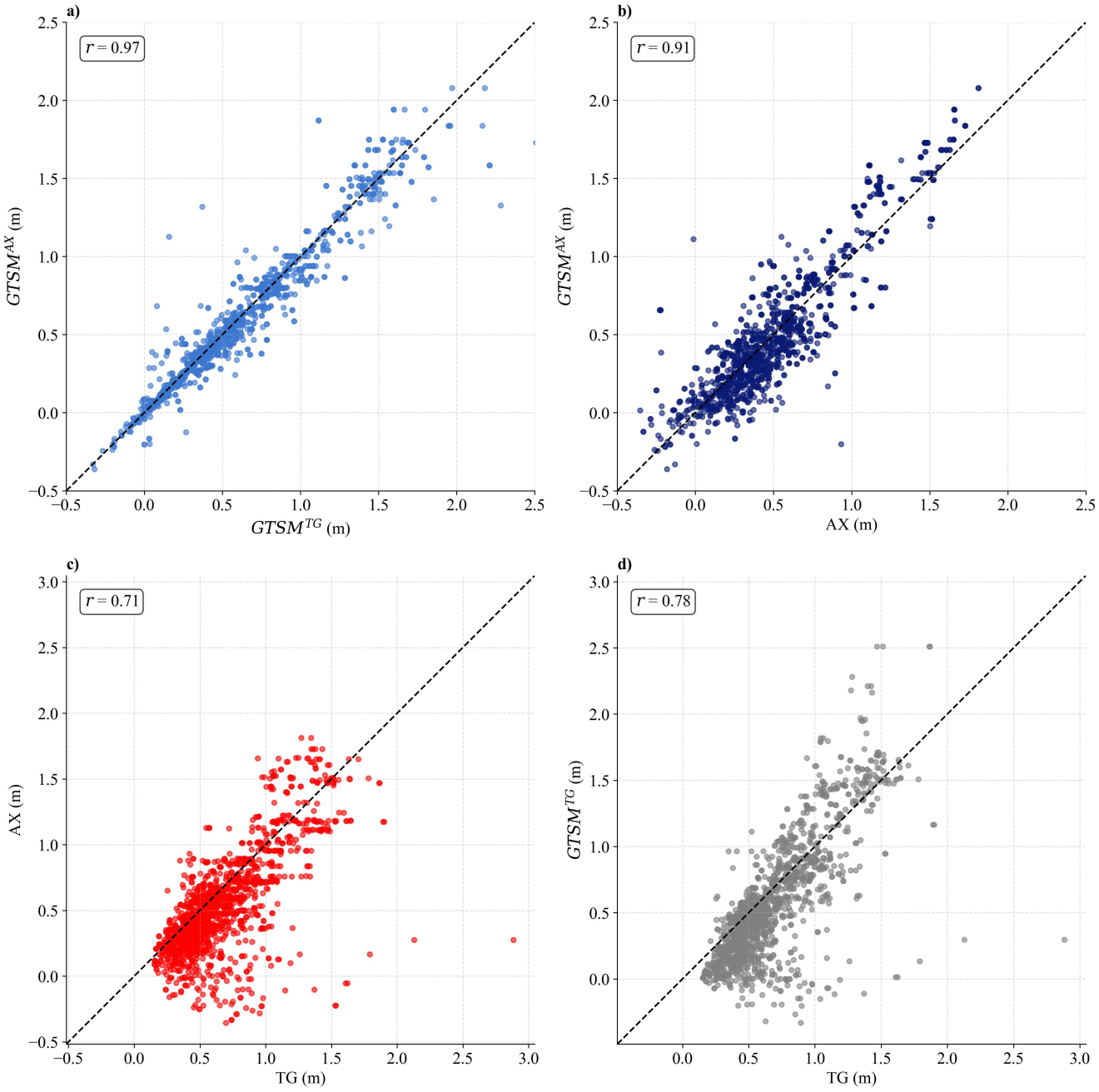


Figure 8. Comparison of storm surge measurements between the GTSM model and AX altimetry and tide gauge (TG). The three panels show (a) GTSM nearest to the altimetry point versus GTSM nearest to the tide gauge, (b) AX versus GTSM nearest to the altimetry point, (c) AX versus the tide gauge, and (d) GTSM nearest to the tide gauge versus the tide gauge. The dashed line indicates 1:1 agreement between the paired measurements.

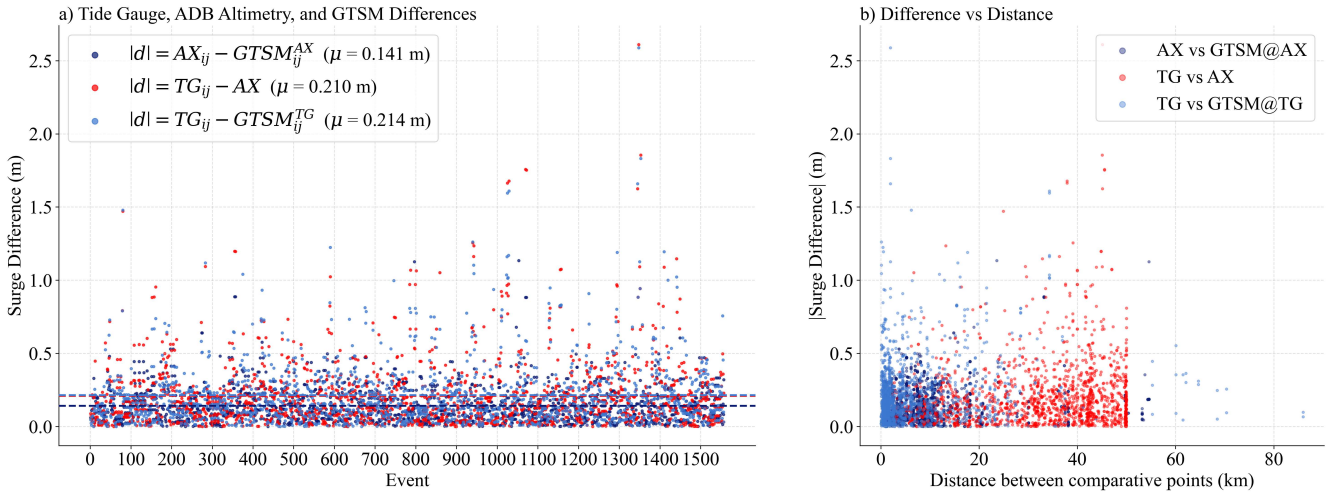


Figure 9. (a) Differences in storm surge estimates between the tide gauge (TG), altimetry (AX), and the nearest GTSM estimate to the altimetry point. (b) Spatial distances between the corresponding comparison points versus differences.

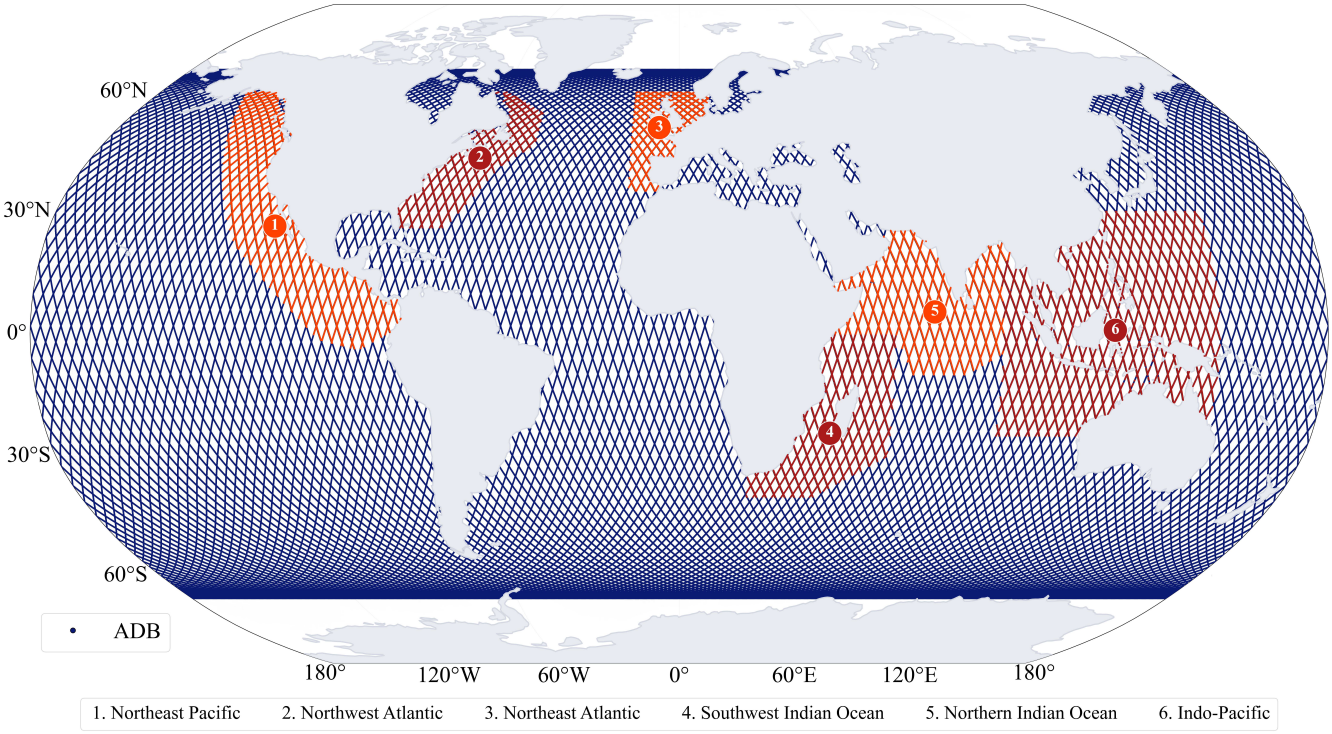


Figure 10. AX (red) and ADB (blue) altimetry data coverage and the six focus regions.

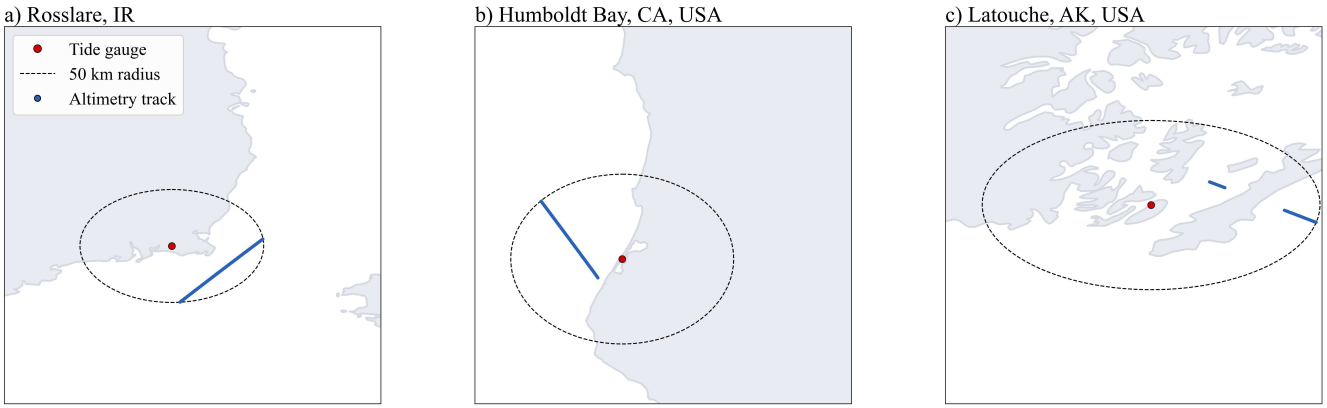


Figure 11. Examples of altimetry track orientation with respect to tide gauges. An example of (a) a parallel track and (b) perpendicular orientation is shown, as well as (c) a complex case with land-shielding and island interference.

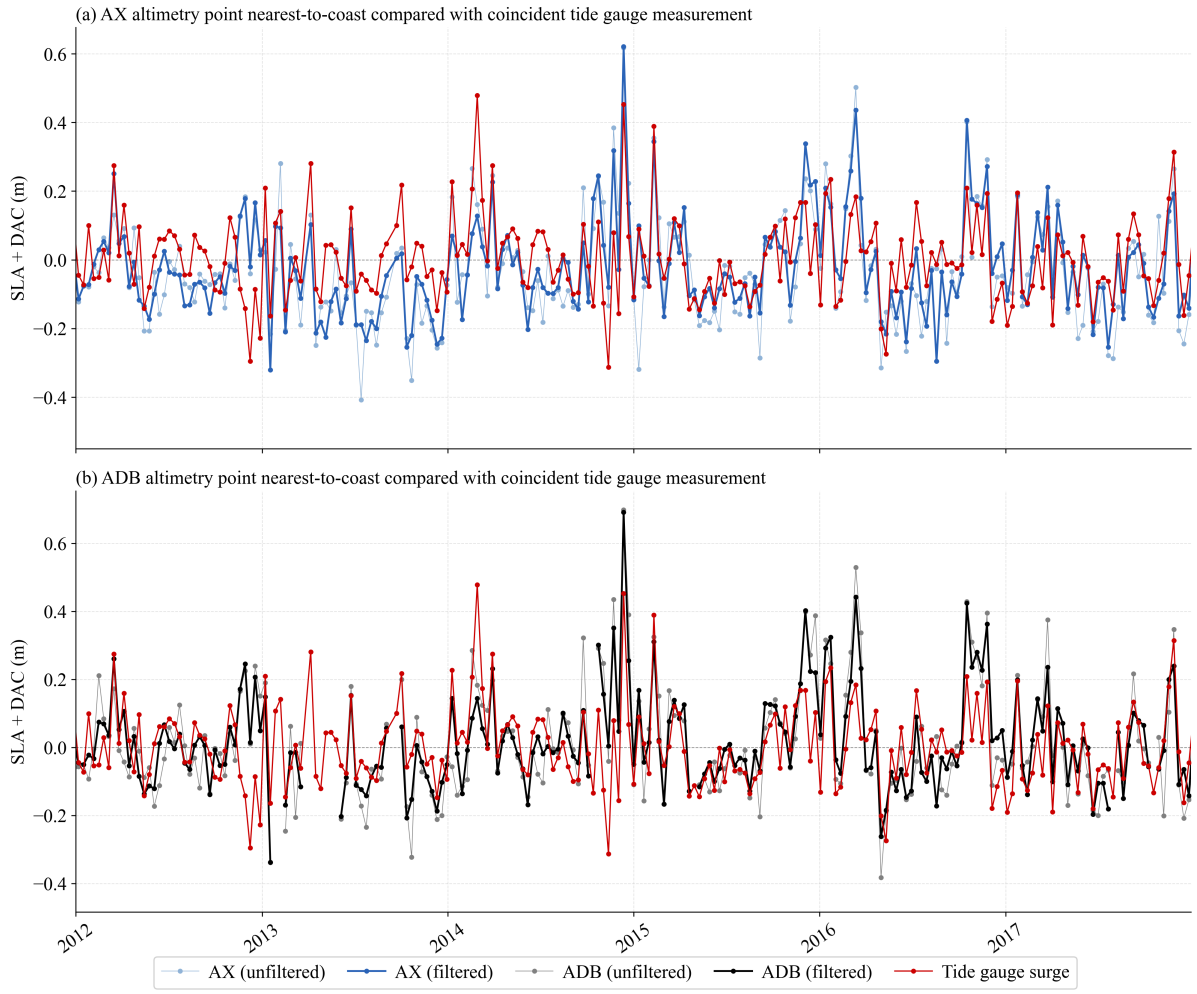


Figure 12. The filtered and unfiltered nearest-to-coast altimetry data for a) AX and b) ADB compared with the coincident Bamfield, BC, CA tide gauge observations.

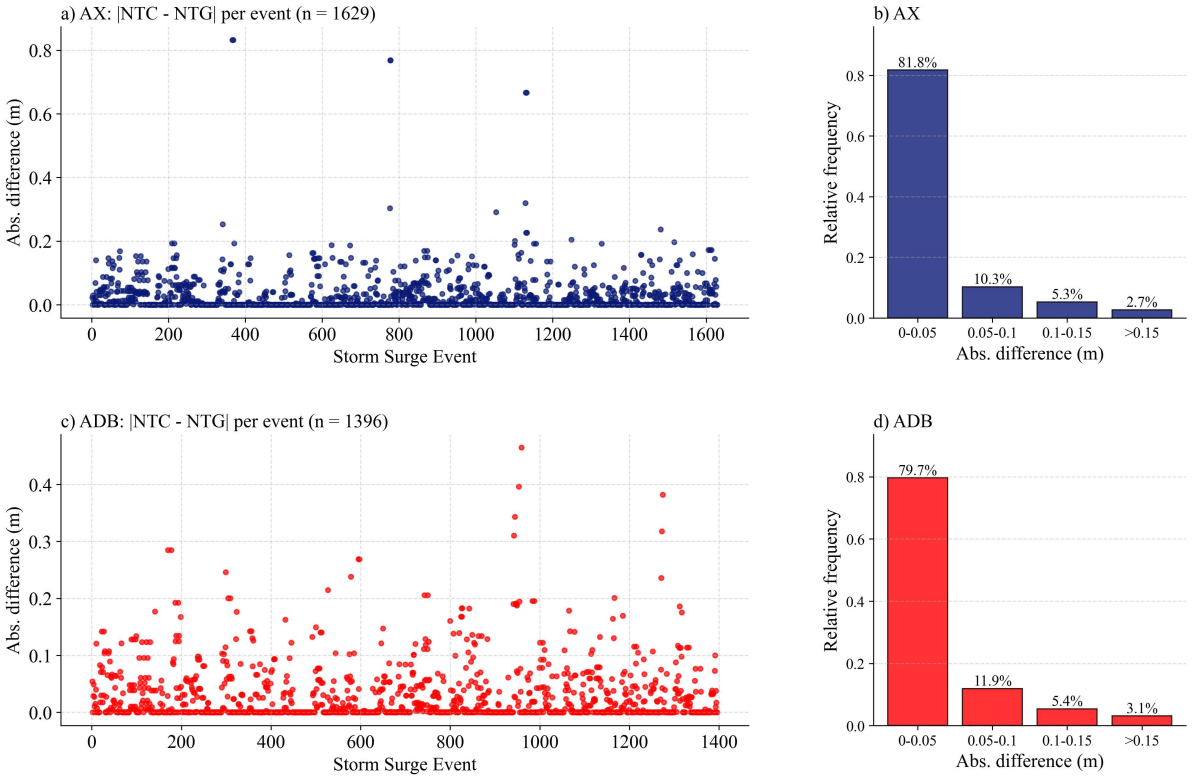


Figure 13. Absolute differences between NTC and NTG SLA+DAC observations at all tide gauge locations for all storm surge events. The upper panel shows the differences for AX NTG relative to NTC, while the lower panel shows the corresponding differences for ADB NTG relative to NTC. The side panels show the relative-frequency histograms of the differences.

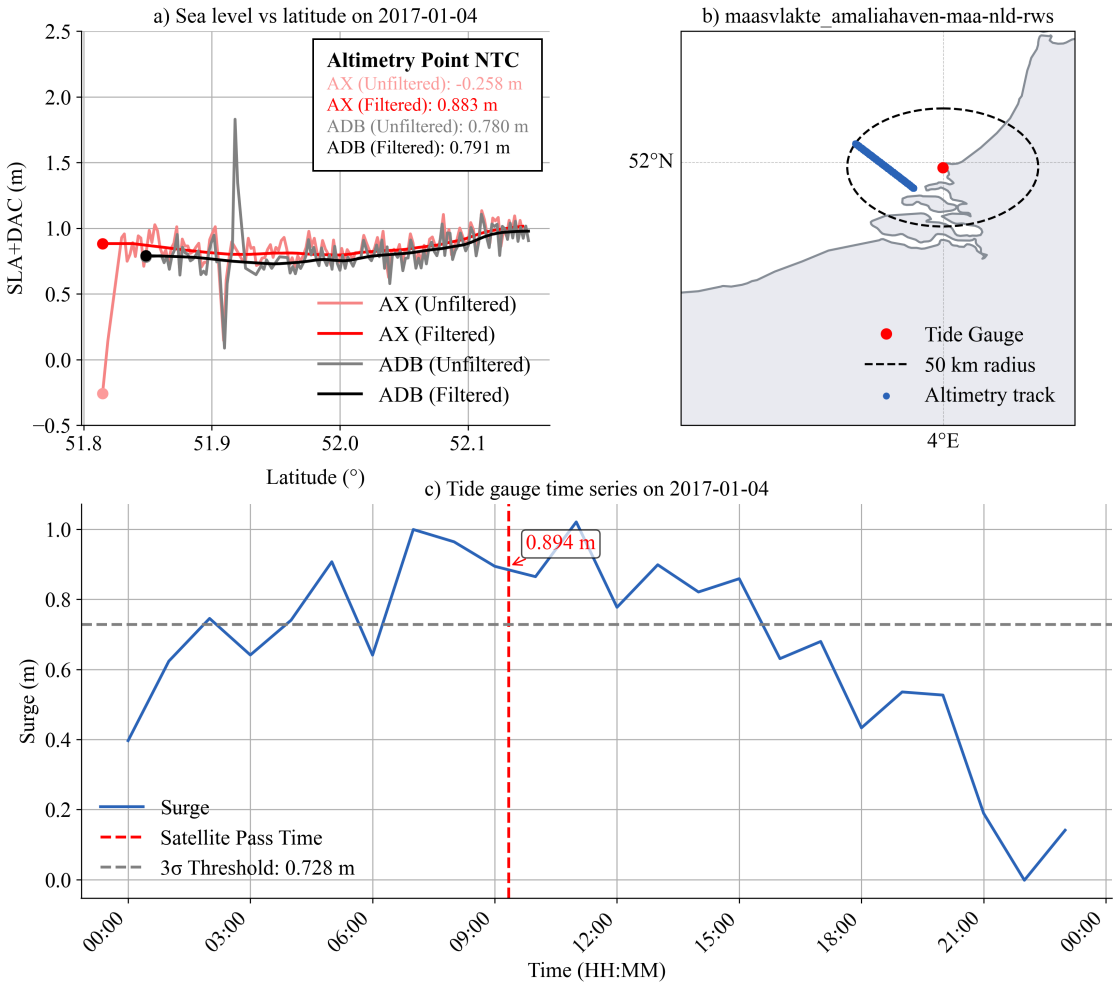


Figure 14. Storm surge identification results for a gauge-altimetry match case in the Netherlands, on 1 April 2017. Implementation of the filter improves the representation of the storm surge signal, reducing outliers and the error between the NTC altimetry observation and the coincident tide gauge measurement.

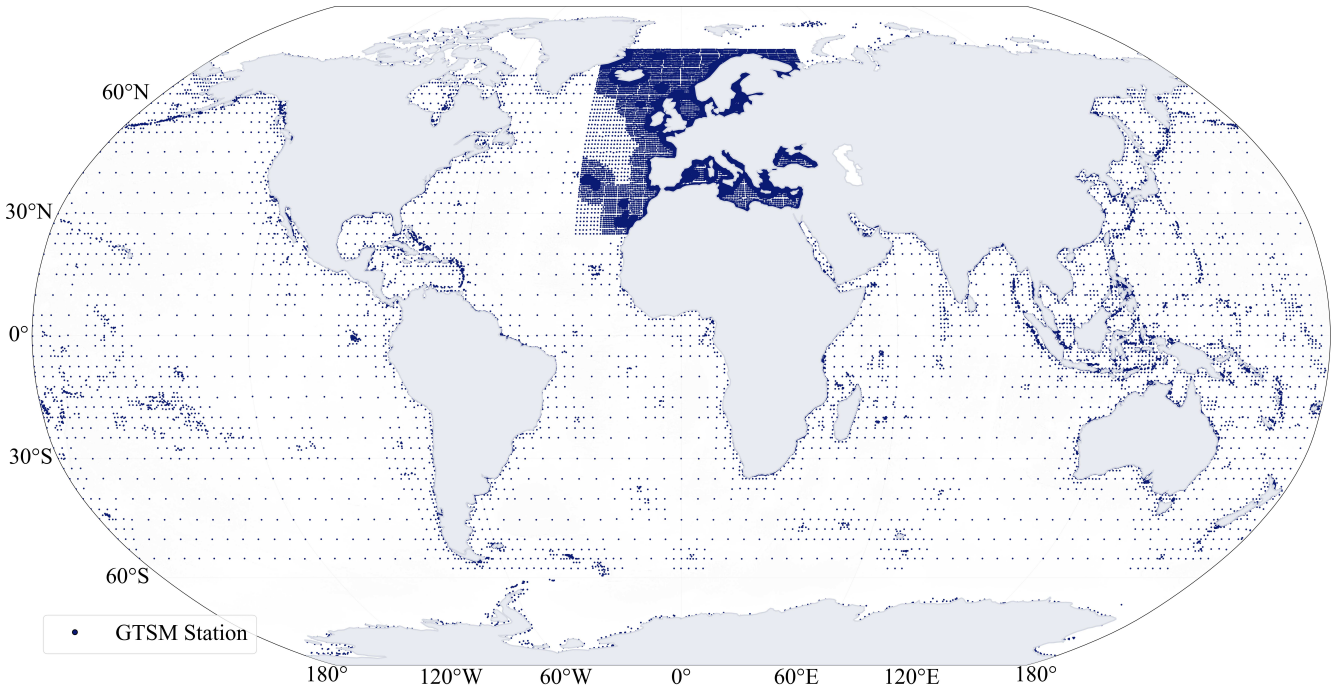


Figure 15. Distribution of GTSM stations.

Supplementary Files

This is a list of supplementary files associated with this preprint. Click to download.

- SupplementaryInformation.tex
- gaugesRawTideGauge.png
- gaugesCorrectedWaterLevel.png
- gaugesPredictedTide.png
- gaugesSurge.png
- mapselectedgaugeszoomed.png
- mumblesvalidatenew41.png
- boobyisland336ausuhslcfdseries.png